



## Control of magma flow in dykes on cyclic lava dome extrusion

A. Costa,<sup>1,2</sup> O. Melnik,<sup>1,3</sup> R. S. J. Sparks,<sup>1</sup> and B. Voight<sup>4</sup>

Received 5 July 2006; revised 23 November 2006; accepted 6 December 2006; published 24 January 2007.

[1] Lava dome eruptions are commonly characterized by large fluctuations in discharge rate with cyclic behaviour on time-scales ranging from hours to decades. Examples include Bezymianny volcano (Russia), Merapi (Java), Santiaguito (Guatemala), Mt St Helens (USA), Mt Unzen (Japan), and Soufrière Hills volcano (Montserrat). Previous models have assumed simple cylindrical conduits for magma transport, but extrusions are mainly fed by dykes, with cylindrical geometries developing only at shallow levels. The widths of dykes embedded in an elastic medium are influenced by local magma pressure, affecting flow rates and system dynamics strongly. We develop a model for magma flow in dykes, which predicts intense pulsations of magma extrusion for the case of a constant source pressure. The period time scale is determined by the elastic deformation of the dyke walls and the length-to-width ratio of the dyke. The dyke acts like a volumetric capacitor, storing magma as pressure increases and then releasing magma in a pulse of extrusion. For the Soufrière Hills volcano, cyclic extrusions with time-scales of a few weeks are predicted for dykes 300–500 m long and 3–6 m wide, matching observations. The model explains the sharp onset of tilt pulsations and seismic swarms. **Citation:** Costa, A., O. Melnik, R. S. J. Sparks, and B. Voight (2007), Control of magma flow in dykes on cyclic lava dome extrusion, *Geophys. Res. Lett.*, 34, L02303, doi:10.1029/2006GL027466.

### 1. Introduction

[2] Many lava dome eruptions are characterized by cyclic patterns of activity on several different time-scales. Well-documented examples include Mount St Helens, USA (1980–1986), Mount Unzen, Japan (1991–1995), Santiaguito dome, Guatemala (1922–present), Merapi, Java (~1883–present), Bezymianny, Russia (1956–present), Mount Pinatubo, Philippines [1991] and Soufrière Hills volcano (SHV), Montserrat (1995–present) [Swanson and Holcomb, 1990; Belousov et al., 2002; Voight et al., 2000; Nakada et al., 1999; Harris et al., 2002; Denlinger and Hoblitt, 1999; Voight et al., 1999]. Commonly several cyclic time-scales are superimposed so a single explanation of cyclicity is unlikely to be satisfactory. Short time-scale cyclicity of several hours to days is characterized by seismicity, inflation and deflation, recognised by tilt data, and eruptive activity [Denlinger and Hoblitt, 1999; Voight et al., 1999]. These short time-scale patterns have been explained

by upper conduit pressurization related to non-linear dynamics of magma flow with stick-slip flow in conduits [Denlinger and Hoblitt, 1999; Voight et al., 1999; Wylie et al., 1999; Ozerov et al., 2003]. Cycles with time-scales of several weeks have also been observed, at Mount St Helens and SHV. In the former case [Swanson and Holcomb, 1990] lava dome extrusion occurred over 2 to 7 days separated by repose periods of 75 to 80 days in 1980–1982. In the latter case an approximately 5 to 7 week cyclic pattern of activity was recognized [Voight et al., 1999; Sparks and Young, 2002] between April 1997 and March 1998 from peaks in the intensity of eruptive activity and geophysical data, including tilt and seismicity (Figure 1).

[3] Pulsations with time scales of six months to decades have also been recognized [Belousov et al., 2002; Voight et al., 2000; Sparks and Young, 2002; Wadge et al., 2006]. Since 1956 eruptions at Bezymianny have occurred once or twice per year [Belousov et al., 2002], at Merapi five voluminous eruptions occurred in the last century [Voight et al., 2000], and in the ongoing SHV eruption there have been three periods of dome extrusion lasting 2 to 3 years separated by quiescent periods of 18 months and 2 years [Sparks and Young, 2002; Wadge et al., 2006; Sparks et al., 1998]. Periods of dome extrusion are accompanied by ground deflation, while quiescent periods are accompanied by ground inflation [Wadge et al., 2006; Mattioli et al., 1998], indicating a link with magma chamber pressure. Recent models have explored magma flows in conduits in dome-forming eruptions supplied from elastic-walled open-system magma chambers [Melnik and Sparks, 1999, 2005; Barmin et al., 2002]. These models can simulate periodic behavior as a consequence of non-linear processes related to degassing, crystallization and rheological stiffening of magma during decompression. Time-scales are in the range of weeks to decades and depend principally on magma rheology, conduit cross-sectional area and the volume of the magma chamber. These models might be applicable to explaining the 2–3 year cycles of dome extrusion at SHV, where deformation data indicate that the magma chamber regulates the cycles, but the models cannot simultaneously explain the 5–7 week cycles. Thus another mechanism is needed.

[4] Models of conduit flow in dome eruptions have assumed a simple cylindrical conduit geometry, and, apart from a study considering short-term oscillatory flow [Wylie et al., 1999], have not considered elastic deformation of the conduit walls. However, there is compelling evidence that domes are fed by dykes, and that cylindrical conduit geometry is only developed at shallow levels, aided by localized flow and explosive activity. For example, surface deformation structures, earthquake locations and continental drilling indicate that the Mount Unzen dome was fed through a dyke [Yamashina and Shimuzu, 1999; Nakada and Eichelberger, 2004], and evidence for a dyke feeder at SHV includes GPS data [Mattioli et al., 1998], distribution

<sup>1</sup>Department of Earth Sciences, University of Bristol, Bristol, UK.

<sup>2</sup>Istituto Nazionale di Geofisica e Vulcanologia, Naples, Italy.

<sup>3</sup>Institute of Mechanics, Moscow State University, Moscow, Russia.

<sup>4</sup>Geosciences, Penn State University, University Park, Pennsylvania, USA.

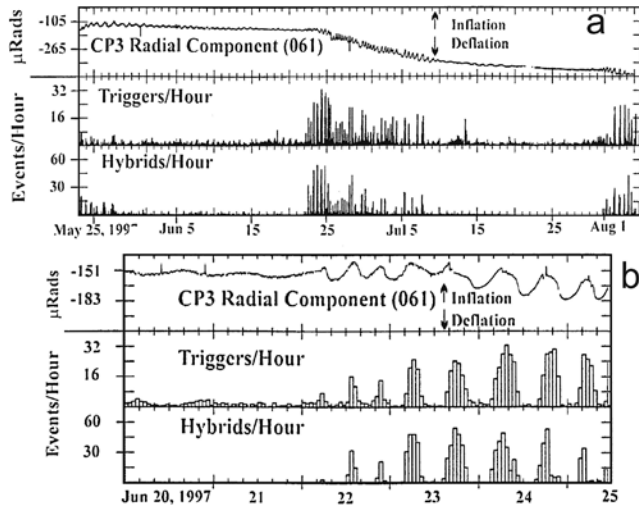


**Figure 1.** (a) Example of cyclic behaviour in a lava dome eruption. Radial tilt, triggered earthquakes, and hybrid earthquakes for 17 May to 6 August 1997, at Soufriere Hills volcano [Voight *et al.*, 1999]. Triggered earthquakes are the number automatically recorded at a given station and are mainly a measure in real-time of hybrid earthquake swarms. Parts of three 5–7 week cycles are shown, with each cycle showing high amplitude tilt and seismicity pulsations with short time scale that last for several weeks after the start of the cycle. The second cycle illustrates well a marked deflation over several weeks that accompanies high discharge. (b) The onset of a cycle is rapid, as detailed here for the cycle initiating on 22 June 1997. The onset is noted by a sharp deflection, a change to shorter period and higher amplitude of tilt pulsations, and swarm seismicity correlated with phase of tilt.

of active vents, and seismic data [Roman *et al.*, 2006]. The width of an elastic-walled dyke changes with pressure [Lister and Kerr, 1991] and the flow rate strongly depends on such changes in dyke width as well as rheological property variations related to decompression, degassing and crystallization. Here we develop a model of lava dome extrusion from a dyke.

[5] The model of Melnik and Sparks [2005] describes magma flow in volcanic conduits during lava dome extrusion. It accounts for degassing-induced crystallization kinetics, gas exsolution and filtration through the magma, rheological stiffening of magma due to crystal growth, and latent heat release. Mass conservation equations for melt, microlites, phenocryst, dissolved and exsolved gas are solved numerically together with an energy equation and two momentum equations (for the mixture as a whole and the gas phase). Here the model has been adapted for the variations in conduit cross-section area due to elastic deformation of the wallrocks. We assume that the conduit has elliptic cross-section with length axes dependent on the vertical coordinates and a transition from a thin dyke at depth to a cylindrical conduit at shallow level (Figure 2). This geometry is chosen because of the observation that the SHV conduit is cylindrical at shallow level [Sparks and Young, 2002; Melnik and Sparks, 2005] due to early explosive eruptions, and is a dyke at depth from

geophysical observations [Mattioli *et al.*, 1998; Roman *et al.*, 2006].

## 2. Governing Equations and Parameter Values

[6] We model the ascent of magma along the conduit ( $x$ -direction) from the chamber with a set of 1D transient equations including mass (1, 2), momentum (3) and energy (4) conservation:

$$\frac{\partial}{\partial t} \rho_m S + \frac{\partial}{\partial x} \rho_m V S = -S(G_{mc} + G_{ph}) \quad (1)$$

$$\frac{\partial}{\partial t} \rho_{ph} S + \frac{\partial}{\partial x} \rho_{ph} V S = G_{ph} S; \quad \frac{\partial}{\partial t} \rho_{mc} S + \frac{\partial}{\partial x} \rho_{mc} V S = G_{mc} S$$

$$\frac{\partial}{\partial t} \rho_d S + \frac{\partial}{\partial x} \rho_d V S = -J S; \quad \frac{\partial}{\partial t} \rho_g S + \frac{\partial}{\partial x} \rho_g V_g S = J S \quad (2)$$

Equations (1) and (2) represent the conservation of mass for melt and crystals (for phenocrysts and microlites) and dissolved and exsolved gas, respectively. Here  $t$  denotes time,  $x$  is the vertical coordinate,  $\rho_m$ ,  $\rho_{ph}$ ,  $\rho_{mc}$ ,  $\rho_d$  and  $\rho_g$  are the densities of melt, phenocrysts, microlites, dissolved and exsolved gas, respectively,  $V$  and  $V_g$  are the velocities of magma and gas,  $S = \pi ab$  is the cross-section area of the conduit ( $a$  and  $b$  are dyke semi-axes),  $G_{ph}$ ,  $G_{mc}$  and  $J$  represent the mass fluxes due to crystallization of

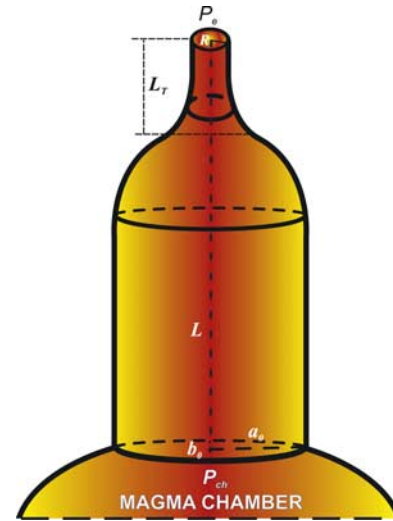


**Figure 2.** Schematic view of volcanic system. A smooth transition from an elliptic dyke to a cylindrical conduit occurs below depth  $L_T$  of approximately 1 km. The chamber is located at 5 km depth. The conduit radius  $R$  is taken as 15 m. The variation with depth of semi-axis lengths,  $a_0$  and  $b_0$ , are defined using arctangent functions. Cross-section of unpressurized dyke is equal to the cross-section of the conduit. Due to high magmatic overpressures (Figure 3) the cross-section area of the elliptic part of the dyke increases significantly with respect to the cross-section area of unpressurized dyke (see Figure 4). At the inlet of the dyke and at the top of the conduit constant pressures ( $P_{ch}$  and  $P_e$ ) are specified as boundary conditions.

**Table 1.** Parameters Used in the Simulations

Notation	Description	Value
$c_0$	concentration of dissolved gas	6 wt%
$C_f$	solubility coefficient	$4.1 \times 10^{-6} \text{ Pa}^{-1/2}$
$C_m$	specific heat	$1.2 \times 10^3 \text{ J kg}^{-1} \text{ K}^{-1}$
$I_0$	max nucleation rate	$3 \times 10^{10} \text{ m}^{-3} \text{ s}^{-1}$
$L^*$	latent heat of crystallization	$3.5 \times 10^5 \text{ J kg}^{-1}$
$P_{ch}$	chamber pressure	160 MPa
$R_g$	gas constant	$460 \text{ J kg}^{-1} \text{ K}^{-1}$
$R_{ph}$	phenocryst size	5 mm
$T_{ch}$	temperature in the magma chamber	860°C
$U_0$	max growth rate	$2 \times 10^{-9} \text{ m s}^{-1}$
$\beta_{ch}^*$	chamber crystal content	0.5
$\mu_{g_0}^0$	gas viscosity	$1.5 \times 10^{-5} \text{ Pa s}$
$\rho_c^0$	density of crystals	$2700 \text{ kg m}^{-3}$
$\rho_m^0$	density of the melt phase	$2300 \text{ kg m}^{-3}$
$\rho_r$	density of wallrocks	$2600 \text{ kg m}^{-3}$

phenocrysts and microlites, and gas exsolution, respectively. These mass fluxes depend on magma undercooling and volatile supersaturation and are calculated based on work by *Melnik and Sparks* [2005]. Because we allow gas filtration through ascending magma two momentum equations are necessary to describe the motion of the mixture. The first momentum equation is for the mixture as a whole in which the pressure decreases due to gravity and conduit resistance calculated for laminar flow in an elliptic pipe, and the second is the Darcy law to describe the exsolved gas flux through the magma:

$$\frac{\partial p}{\partial x} = -\rho g - 4\mu \frac{a^2 + b^2}{a^2 b^2} V; \quad V_g - V = -\frac{k(\alpha)}{\mu_g} \frac{\partial p}{\partial x} \quad (3)$$

Here  $\rho$  is the bulk density of erupting magma,  $p$  is the pressure,  $g$  is the gravity acceleration,  $\mu$  is the magma viscosity,  $k$  is the magma permeability and  $\mu_g$  is the gas viscosity. Permeability is assumed to depend only on bubble volume fraction  $\alpha$  [e.g., *Costa*, 2006] and empirically described as  $k(\alpha) = k_0 \alpha^j$  (with  $k_0 = 5 \times 10^{-12} \text{ m}^2$  and  $j = 3.5$ ).

[7] The thermal energy equation accounting for release of latent heat of crystallisation is given by;

$$\frac{\partial}{\partial t} \rho_{cond} C_m T S + \frac{\partial}{\partial x} \rho_{cond} C_m T V S = S [L^* (G_{ph} + G_{mc}) - T J];$$

$$\rho_{cond} = \rho - \rho_g \quad (4)$$

Here  $T$  is the temperature,  $C_m$  is the heat capacity of magma, and  $L^*$  is the latent heat of crystallization, which are assumed to be constant.

[8] Extra equations are necessary to relate densities in equations (1) and (2) with volume concentrations of bubbles and crystals (phenocrysts and microlites) and mass fraction of dissolved gas. As an equation of state perfect gas law is assumed for exsolved gas, melt and crystals are assumed to be incompressible. Parameter definition and values are given in Table 1. They are either the same or similar to those used by *Melnik and Sparks* [2005], so that the model predictions can be compared with a well-documented study and effects due to the dyke geometry can be easily identified. Magma viscosity is modeled as a product of melt viscosity  $\mu_m(c, T)$  calculated after *Hess and Dingwell* [1996] where  $c$  is mass fraction of dissolved volatiles, here assumed to be water, relative viscosity due to the presence of crystals  $\theta(\beta)$ , and relative

viscosity due to the presence of bubbles  $\eta(\alpha, Ca)$ :  $\mu = \mu_m(c, T)\theta(\beta)\eta(\alpha)$ . Viscosity increase due to the crystals is introduced as following [*Costa*, 2005] (further comments available at <http://arxiv.org/abs/physics/0512173>):

$$\theta = \frac{1 + \left(\frac{\beta}{\beta_*}\right)^\delta}{\left(1 - \text{erf}\left\{\frac{\sqrt{\pi}}{2\varepsilon} \frac{\beta}{\beta_*} \left[1 + \left(\frac{\beta}{\beta_*}\right)^\gamma\right]\right\}\right)^{2.5\beta_*}} \quad (5)$$

where  $\beta_*$  represents the critical transition fraction,  $\varepsilon$  ( $0 < \varepsilon < 1$ ) determines the value of  $\theta(\beta_*)$  ( $\varepsilon$  can be obtained from  $\theta(\beta_*) = 2 \times [1 - \text{erf}(\sqrt{\pi}/\varepsilon)]^{-2.5\beta_*}$ ),  $\gamma$  controls the steepness of the rheological transition, and  $\delta$  controls the increase of  $\theta$  as  $\beta \rightarrow 1$ . In principle  $\beta_*$ ,  $\gamma$ ,  $\delta$  and  $\varepsilon$  can be functions of the strain rate and crystal shape but here are assumed to be constant (we use  $\beta_* = 0.67$ ,  $\gamma = 3.99$ ,  $\delta = 16.94$  and  $\theta(\beta_*) = 3288$ ). Effects due to the presence of bubbles are treated by adopting a generalization of *Llewellyn and Manga* [2005]:

$$\eta(\alpha, Ca) = \frac{1}{1 + 25Ca^2} \left[ \frac{1}{(1 - \alpha)} + 25Ca^2(1 - \alpha)^{5/3} \right] \quad (6)$$

where  $Ca = \lambda \dot{\gamma}$  is the capillary number,  $\lambda$  a characteristic bubble time scale [*Llewellyn and Manga*, 2005] and  $\dot{\gamma}$  is the shear strain-rate averaged on the elliptical cross section.

[9] Lengths of the dyke semi-axes  $a$  and  $b$  depend on magmatic overpressure  $\delta p$  as follows [*Mériaux and Jaupart*, 1995]:

$$a(x, t) = a_0(x) + \frac{\delta p(x, t)}{2G(x)} [-(1 - 2\nu)a_0(x) + 2(1 - \nu)b_0(x)]$$

$$b(x, t) = b_0(x) + \frac{\delta p(x, t)}{2G(x)} [2(1 - \nu)a_0(x) - (1 - 2\nu)b_0(x)]. \quad (7)$$

[10] Here  $\delta p$  is the overpressure, *i.e.* the difference between conduit pressure and far field pressure here assumed lithostatic for a sake of simplicity,  $G$  is the rigidity of wall-rock,  $\nu$  is Poisson's ratio,  $a_0$  and  $b_0$  are the unpressurized values of the semi-axes. The value of  $a_0$  with depth is parameterized as:  $a_0(x) = A_1 \arctan\left(\frac{x-L_T}{w_T}\right) + A_2$ , where  $L_T$  and  $w_T$  are the position and the vertical extent of the

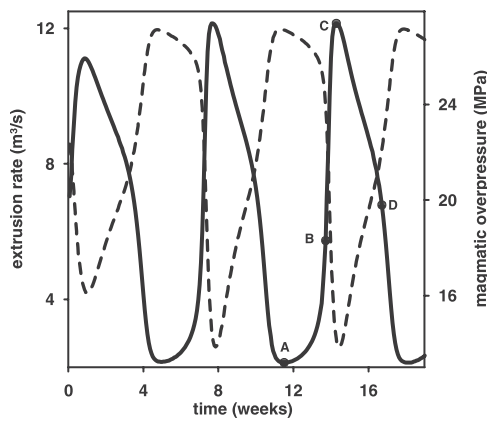


**Figure 3.** Dependence of magma discharge rate (solid line) and magmatic overpressure at depth of 1 km (dashed line) on time, for  $a = 240$  m and  $b = 2.25$  m at the inlet of the dyke. The period of cycle is 46 days, average discharge rate is  $6.2 \text{ m}^3/\text{s}$ , with peak rate about  $12 \text{ m}^3/\text{s}$ . Four points labeled show positions within a cycle of the dyke cross-section profiles in Figure 4.

transition zone and constants  $A_1$  and  $A_2$  are calculated to satisfy conditions  $a_0(L) = R$  and  $a_0(0) = a_0$ . The value of  $b_0$  is calculated to conserve the cross-section area of the unpressurized dyke, although it can also be specified independently. The depth of the transition from dyke to cylinder  $L_T$  is not well-constrained, but here is assumed to be 1 km. Depth to the chamber  $L$  is taken as 5 km, and upper conduit radius  $R$  is taken as 15 m. Rigidity values in volcanic systems are uncertain due to the presence of fractures and high temperatures. Both measurements in laboratory [Voight *et al.*, 1999] and best-fits for ground deformation [Voight *et al.*, 2006; Beauducel *et al.*, 2000] and seismicity [Troise *et al.*, 2003] suggest a range of 1 GPa to 5 GPa. A linear variation of  $G$  with depth from 1.5 GPa at the surface to 6 GPa at 5 km is assumed. A Poisson ratio  $\nu = 0.3$  was used.

[11] A parametric study for investigating the sensitivity of the set of non-linear equations (1)–(7) to the controlling parameters, such as physical parameters related with magma properties [e.g., Melnik and Sparks, 2005] and geometrical parameters related with the conduit shape is outside the scope of this paper due to space limits and is the subject of other ongoing studies.

### 3. Results and Discussion

[12] The time-average discharge rate in April 1997 to March 1998 period at SHV was 5 to  $7 \text{ m}^3/\text{s}$ , with 7 cycles lasting between 30 and 52 days [Sparks and Young, 2002]. The average magma volume extruded during one cycle was approximately  $0.02\text{--}0.03 \text{ km}^3$ . This volume is much less than the estimated chamber volume of about  $4\text{--}5 \text{ km}^3$  [Voight *et al.*, 2006]. Extrusion of magma will, thus, lead to less than 5 MPa pressure variations inside the magma chamber. This allows us to keep chamber pressure constant. We have validated this assumption by running models with and without magma chamber coupling.

[13] A new result is that, even with a fixed chamber pressure, there are discharge rate oscillations. At the beginning of a cycle the discharge rate is at a minimum while the overpressure and dyke width are at a maximum (Figures 3

and 4). At point A in Figure 3 the crystal content and viscosity have reached their maximum values. Beyond this threshold condition an increase in discharge rate results in decreasing pressure and dyke width. However, crystal content and viscosity also decrease and this effect decreases friction, resulting in flow rate increase and pressure decrease. At C the system reaches a minimum in viscosity and crystal content, which cannot decline further. Thereafter the discharge rate decreases, while the pressure and dyke width increase. The dyke acts like a capacitor in storing volume during this part of the cycle.

[14] The period of oscillations depends on several parameters such as influx rate and dyke aspect ratio  $a/R$ . Typically the period decreases with larger aspect ratios. The range of calculated periods varies between 38 and 51 days for major semi-axis lengths  $a$  from 175 to 250 m and minor semi-axes  $b$  from 2 to 4 m. These results match observed cyclicity at SHV. The start of cycle is quite sharp (Figure 1), with onset of shallow hybrid-type (impulsive, low-frequency coda) earthquakes. The change to shorter period and higher amplitude tilt pulsations indicates a marked increase in average magma discharge rate [Voight *et al.*, 1999; Wylie *et al.*, 1999]. The model cycles also have rapid onsets. The high-amplitude tilt pulsations lasted for several weeks [Voight *et al.*, 1999], consistent with the duration of higher discharge rates early in each 5–7 week cycle (cf. Figures 1 and 3). Tilt data (Figure 1) are consistent with the model in that the episode of high discharge is associated with a marked deflation that lasts several weeks. The magma pressure builds up in the swelling dyke and then reaches a threshold, whereupon a surge of partly crystallized magma occurs accompanied by elevated seismicity. Similarly, the 75 to 80 day cycles at Mount St

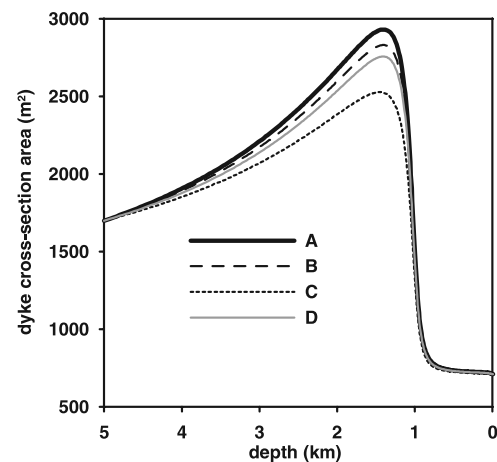


**Figure 4.** Profiles of cross-section areas of the conduit during one cycle. Curve A corresponds to the beginning of the cycle (see Figure 3), B - to a point on the curve of ascending discharge rate, C - to maximum discharge, and D to the middle of descending discharge curve. At the beginning of the cycle, due to large viscosity of magma (at low discharge rate crystal content is high) large magmatic overpressure develops, reaching a maximum near the transition between the dyke and cylindrical conduit; the dyke inflates providing temporary magma storage. Minimum dyke volume corresponds to maximum discharge rate (curve C).

Helens in 1980–1982 [Swanson and Holcomb, 1990] had rapid onsets, characterized by rapidly accelerating ground deformation and shallow seismicity followed by a short pulse of dome extrusion. The model cycles can be made sharper and shorter with periods of quiescence, as at Mount St Helens, by taking into account non-Newtonian magma rheology [Melnik and Sparks, 2005]. Dykes embedded in elastic media can cause strongly pulsed extrusion of magma, with the period time scale being determined by the elastic properties of the dyke walls and the length-to-width ratio of the dyke. For a well-constrained case (SHV) cyclic pulsations can therefore exhibit multiple regimes, one characterized by chamber dynamics [Melnik and Sparks, 2005], and the other by dyke dynamics; the model is able to replicate the enigmatic 5–7 week cycles observed at SHV and explains the sharp onset of tilt pulsations and earthquakes. Our results draw attention to the sensitive dynamic role played by dyke conduits in eruptive systems. These results have strong implications for hazards management, as the anticipation of sharp and possibly explosive onsets at volcanoes with cyclic activity can be used to develop hazards mitigation strategies in advance.

[15] **Acknowledgments.** The authors acknowledge NERC grants (NE/C509958/1) and support from the Royal Society International collaboration fund. RSJS acknowledges a Royal Society-Wolfson Merit Award, OEM acknowledges support from Russian Foundation for the Basic Research (05-01-00228) and BV acknowledges support from NSF Earth Sciences.

## References

- Barmin, A., O. Melnik, and R. S. J. Sparks (2002), Periodic behavior in lava dome eruptions, *Earth Planet. Sci. Lett.*, *199*, 173–184.
- Beauducel, F., F. H. Cornet, E. Suhanto, T. Duquesnoy, and M. Kasser (2000), Constraints on magma flux from displacements data at Merapi volcano, Java, Indonesia, *J. Geophys. Res.*, *105*(B4), 8193–8203.
- Belousov, A., B. Voight, M. Belousova, and A. Petukhin (2002), Pyroclastic surges and flows from the 8–10 May 1997 explosive eruption of Bezmyanny volcano, Kamchatka, Russia, *Bull. Volcanol.*, *64*, 455–471.
- Costa, A. (2005), Viscosity of high crystal content melts: Dependence on solid fraction, *Geophys. Res. Lett.*, *32*, L22308, doi:10.1029/2005GL024303.
- Costa, A. (2006), Permeability-porosity relationship: A re-examination of the Kozeny-Carman equation based on fractal pore-space geometry, *Geophys. Res. Lett.*, *33*, L02318, doi:10.1029/2005GL025134.
- Denlinger, R., and R. P. Hoblitt (1999), Cyclic eruptive behavior of silicic volcanoes, *Geology*, *27*, 459–462.
- Harris, A. J. L., W. I. Rose, and L. P. Flynn (2002), Temporal trends in lava dome extrusion at Santiaguito 1922–2000, *Bull. Volcanol.*, *65*, 77–89.
- Hess, K. U., and D. B. Dingwell (1996), Viscosities of hydrous leucogranite melts: A non-Arrhenian model, *Am. Mineral.*, *81*, 1297–1300.
- Lister, J. R., and R. C. Kerr (1991), Fluid mechanical models of crack propagation and their application to magma transport in dykes, *J. Geophys. Res.*, *96*, 10,049–10,077.
- Llewellyn, E. W., and M. Manga (2005), Bubble suspension rheology and implications for conduit flow, *J. Volcanol. Geotherm. Res.*, *143*, 205–217.
- Mattioli, G., T. H. Dixon, F. F. Farina, E. S. Howell, P. E. Jansma, and A. L. Smith (1998), GPS measurement of surface deformation around Soufrière Hills volcano, Montserrat from October 1995 to July 1996, *Geophys. Res. Lett.*, *25*, 3417–3420.
- Melnik, O., and R. S. J. Sparks (1999), Nonlinear dynamics of lava dome extrusion, *Nature*, *402*, 37–41.
- Melnik, O., and R. S. J. Sparks (2005), Controls on conduit magma flow dynamics during lava dome building eruptions, *J. Geophys. Res.*, *110*, B02209, doi:10.1029/2004JB003183.
- Mériaux, C., and C. Jaupart (1995), Simple fluid dynamics models of volcanic rift zones, *Earth Planet. Sci. Lett.*, *136*, 223–240.
- Nakada, S., and J. C. Eichelberger (2004), Looking into a volcano: Drilling Unzen, *Geotimes*, *49*(3), 14–17.
- Nakada, S., H. Shimizu, and K. Ohta (1999), Overview of the 1990–1995 eruption at Unzen Volcano, *J. Volcanol. Geotherm. Res.*, *89*, 1–22.
- Ozerov, A., I. Ispalotov, and J. Lees (2003), Modeling Strombolian eruptions of Karymsky volcano, Kamchatka, Russia, *J. Volcanol. Geotherm. Res.*, *122*, 265–280.
- Roman, D. C., J. Neuberg, and R. R. Lueck (2006), Assessing the likelihood of volcanic eruption through analysis of volcanotectonic earthquake fault-plane solutions, *Earth Planet. Sci. Lett.*, *248*, 244–252, doi:10.1016/j.epsl.2006.05.029.
- Sparks, R. S. J., and S. R. Young (2002), The eruption of Soufrière Hills volcano, Montserrat (1995–1999): Overview of scientific results, *Mem. Geol. Soc.*, *21*, 45–69.
- Sparks, R. S. J., et al. (1998), Magma production and growth of the lava dome of the Soufrière Hills volcano, Montserrat: November 1995 to December 1997, *Geophys. Res. Lett.*, *25*, 3421–3424.
- Swanson, D. A., and R. T. Holcomb (1990), Regularities in growth of the Mount St. Helens dacite dome 1980–1986, in *Lava Flows and Domes: Emplacement Mechanisms and Hazards Implications*, edited by J. H. Fink, pp. 3–24, Springer, New York.
- Troise, C., F. Pingue, and G. De Natale (2003), Coulomb stress changes at calderas: Modeling the seismicity at Campi Flegrei (southern Italy), *J. Geophys. Res.*, *108*(B6), 2292, doi:10.1029/2002JB002006.
- Voight, B., et al. (1999), Magma flow instability and cyclic activity at Soufrière Hills Volcano, Montserrat, *Science*, *283*, 1138–1142.
- Voight, B., E. K. Constantine, S. Siswoidjono, and R. Torley (2000), Historical eruptions of Merapi Volcano, central Java, Indonesia, 1768–1998, *J. Volcanol. Geotherm. Res.*, *100*, 69–138.
- Voight, B., et al. (2006), Unprecedented pressure increase in deep magma reservoir triggered by lava-dome collapse, *Geophys. Res. Lett.*, *33*, L03312, doi:10.1029/2005GL024870.
- Wadge, G., G. S. Mattioli, and R. A. Herd (2006), Ground deformation at Soufrière Hills volcano, Montserrat during 1998–2000 measured by radar interferometry and GPS, *J. Volcanol. Geotherm. Res.*, *152*, 157–173.
- Wylie, J. J., B. Voight, and J. A. Whitehead (1999), Instability of magma flow from volatile-dependent viscosity, *Science*, *285*, 1883–1885.
- Yamashina, K., and H. Shimizu (1999), Crustal deformation in the mid-May 1991 crisis preceding the extrusion of a dacite lava dome at Unzen volcano, Japan, *J. Volcanol. Geotherm. Res.*, *89*, 43–55.

A. Costa, O. Melnik, and R. S. J. Sparks, Department of Earth Sciences, University of Bristol, Wills Memorial Building, Queen's Road, Bristol BS8 1RJ, UK.

B. Voight, Geosciences, Penn State University, University Park, PA 16802, USA.